THE JOURNAL OF PHYSICAL CHEMISTRY C

Article

Cite This: J. Phys. Chem. C 2019, 123, 5023−5030

pubs.acs.org/JPCC

In Situ Growth of Bi Nanoparticles on $NaBiO_3$, δ-, and β-Bi_2O_3 Surfaces: Electron Irradiation and Theoretical Insights

Marcelo Assis,[†] Marisa Carvalho de Oliveira,[‡] Thales Rafael Machado,[†] Nadia Guerra Macedo,[†] João Paulo Campos Costa,[†] Lourdes Gracia,[‡] Juan Andrés,*[,‡] and Elson Longo[†]

[†]CDMF, LIEC, Federal University of São Carlos (UFSCar), P.O. Box 676, São Carlos 13565-905, São Paulo, Brazil

[‡]Department of Analytical and Physical Chemistry, University Jaume I (UJI), Castelló 12071, Spain

Supporting Information

ABSTRACT: Herein, we present a combined experimental and theoretical study of the in situ growth of Bi nanoparticles on $NaBiO_3$, δ-, and β-Bi_2O_3 surfaces mediated by the electron beam of a high-resolution transmission electron microscope. Density functional theory and quantum theory of atoms in molecule calculations were used to gain a deeper insight into the experimental observations and to provide an atomistic basis for understanding the formation mechanism of Bi NPs on $NaBiO_3$, δ-, and β-Bi_2O_3 under electron beam irradiation. Analysis of the experimental data and electron density distributions suggests that the formation of Bi NPs can be related to the structural and electronic changes occurring within the octahedral $[BiO_6]$ clusters, and to a lesser extent, $[NaO_6]$ clusters, which serve as the constituent building blocks of $NaBiO_3$. Our findings indicate that as a function of the number of added electrons, the formation of β-Bi_2O_3 takes place first followed by the subsequent appearance of metallic Bi NPs generated in the crystal by electron beam irradiation.

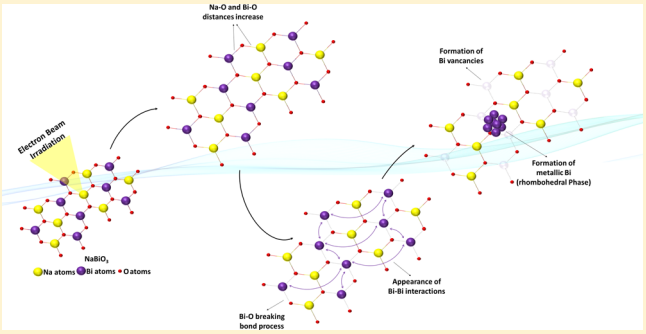

1. INTRODUCTION

The properties derived from the interactions of electrons/waves with matter are of great importance in modern science and engineering. Electron beam irradiation is a necessary and promising area of research because of its wide usage and unique advantages. Furthermore, it is known to be an effective technique for changing or modifying materials; the scattered electrons exiting the back surface of the specimen are a rich source of information about the microstructure and electronic structure of the sample, which can be analyzed based on a variety of electron−solid interaction mechanisms.[1−3]

Conventional techniques for characterizing the microstructure of nanomaterials rely heavily on electron microscopy techniques, in which high-energy electrons are transmitted through the specimen and provide useful information at the nanometer and sub-nanometer levels based on a variety of electron−solid interactions.[4] The electron beam generated within a transmission electron microscope (TEM) or field emission-TEM (FE-TEM) interacts with the sample during imaging and is also a very powerful tool for the fabrication and manipulation of nanostructures with the advantage of precise control at the nanoscale or single nanoparticle (NP) level.[5,6] This is because in a vacuum chamber, despite recent developments in liquid-cell and in situ electron microscopy, the high-energy beam used in an electron microscope is unaffected by chemicals in the surrounding environment, such as solvents, reactants, and electrolytes, which can play an essential role in regulating the chemical activity.[7−9] TEM can be used to fabricate unique highly dispersed nanomaterials by electron beam irradiation, and Böhler et al.[10] reviewed how low-energy electron irradiation is capable of initiating the synthesis of NPs and modifying surfaces with metal NPs. Very recently, Rümmeli et al.[1] reviewed the body of work available on electron-beam-induced synthesis techniques with in situ capabilities.

A tremendous amount of research effort has been devoted to the synthesis of metal NPs on the surfaces of different substrates as they may possess innovative properties and hold great promise for future technology.[11,12] In particular, arrays of metal NPs deposited on surfaces offer great potential for the design of novel nanomaterials for applications in areas such as catalysis, electronic nanodevices, information storage, and quantum computers.[13−18] Thus, it is crucial to investigate the mechanisms governing the formation and modification of metal NPs during characterization under electron beam irradiation.

Our research group have proven that through electron beam irradiation under Ag-based oxides such as α-Ag_2WO_4,[19−27] β-Ag_2WO_4,[28,29] Ag_2CrO_4,[30] Ag_2MoO_4,[31] β-$AgVO_3$,[32] and Ag_3PO_4,[33] Ag NPs can be obtained on the surface of these materials. Other metal NPs were also obtained with electron beam irradiation, such as Li,[34] Cu,[35] Co,[36] and Au,[37] with their

Received: December 1, 2018
Revised: January 26, 2019
Published: February 4, 2019

DOI: 10.1021/acs.jpcc.8b11566
J. Phys. Chem. C 2019, 123, 5023−5030

formation being dependent on the electron beam acceleration voltage, the irradiation time, and the nature of the material to be irradiated, among other factors. Even very recently, we have shown the formation and coexistence of different crystallographic phases (rhombohedral, monoclinic, and cubic) of Bi NPs synthesized by femtosecond radiation in air.[38] As a continuation of these works, in the current investigation, we demonstrate that an electron beam can be used for the formation of Bi NPs on the surface of $NaBiO_3$.

Previously, Jose-Yacaman et al.[39] reported the formation of metallic Bi NPs by focusing a TEM electron beam over $NaBiO_3$. Very recently, Zhang et al.[40] observed the formation of Bi NPs by electron irradiation of $NaBi(MoO_4)_2$ nanosheets at observable conditions (200 kV) in a TEM. While Li et al.[41] managed to unravel the in situ atomic-scale mechanism of crystal nucleation and growth of Bi NPs under an electron beam inside an aberration-corrected TEM. Electrons interact with solids at the quantum level, and improving our understanding and predicting the response of a material to the passage of electrons is critical for various applications but remains a challenging problem. Several questions remain regarding the structural evolution of the crystal lattice during electron irradiation. Bi NPs were also produced by Bi metallic targets in solvents through laser ablation, obtaining spherical NPs of rhombohedral Bi with size range between 60 and 5 nm, the size being dependent on the aperture of the laser spot size, wavelength and laser power, pulse numbers, time slot, and solvent employed, among other factors.[42−44]

To reproduce the experimental scenario as closely as possible, density functional theory (DFT) calculations using the quantum theory of atoms in molecules (QTAIM) were carried out to gain atomistic insights into the in situ growth and structural and electronic evolution of Bi NPs in the $NaBiO_3$ crystal, as defined by the changes in the electron density. Experimental techniques such as high-resolution transmission electron microscopy (HR-TEM) were used. Energy-dispersive X-ray spectroscopy (EDS) was also employed. The results provide a valuable probe into the relationship between atomic-scale structural and electronic perturbations.

Our manuscript is organized as follows: the employed experimental techniques and theoretical methods used to model the bulk systems are described, then, the results are presented and discussed, and we finally conclude with our main findings and implications for future work.

2. METHODS

2.1. Experimental Procedures. Sodium bismuthate ($NaBiO_3$, 80%, Neon) with a δ-Bi_2O_3 impurity (see in the Supporting Information, Figure S1) and bismuth(III) oxide (β-Bi_2O_3, 99.999%, Sigma-Aldrich), both commercial reagents, were used for the experiments. A Jem-2100 LaB6 (JEOL) high-resolution TEM with an accelerating voltage of 200 kV coupled with an INCA Energy TEM 200 (Oxford) energy dispersive X-ray spectrometer was used to irradiate the sample with electrons after depositing small amounts of the powders directly onto carbon-coated Cu grids, while pellets were prepared by ultrasonic dispersion. In addition, we used the same equipment for performing TEM and microanalysis measurements to characterize the structural changes of the samples. The mesh size of TEM grids is 300.

2.2. Theoretical Methods. First-principles total energy calculations were carried out within the periodic DFT framework using the VASP program.[45] The Kohn−Sham equations were solved by means of the Perdew, Burke, and Ernzerhof exchange−correlation functional and the electron−ion interaction described by the projector-augmented-wave pseudopotentials.[46,47] Because of the well-known limitations of standard DFT in describing the electronic structures of "strongly-correlated" compounds, a correction to the PBE wave function was made (PBE + U) by including a repulsive on-site Coulomb interaction, U, according to the formula of Dudarev et al.[48] The orbital dependence of the Coulomb and exchange interactions has been taken into account with this scheme, using a value of 6 eV for the Hubbard parameter for Bi (previously tested). The plane-wave expansion was truncated at a cutoff energy of 520 eV and the Brillouin zones were sampled through Monkhorst−Pack special k-point grids that ensured geometrical and energetic convergence for the $NaBiO_3$, β-Bi_2O_3, and δ-Bi_2O_3 structures considered in this work. In the calculations, electrons were introduced one by one up to eight in the unit cell (keyword NELECT) and the distribution of these extra electrons takes place by means of a simultaneous geometry optimization on both the lattice parameters and the atomic positions. The relationship between charge density topology and elements of molecular structure and bonding was noted by Bader.[49] This relationship, Bader's QTAIM theory,[50,51] is now a well-recognized tool for analyzing electron density, describing interatomic interactions and rationalizing chemical bonding, as used in previous works.[23,26,28,30,32,33,52,53]

3. RESULTS AND DISCUSSION

The unit cell of $NaBiO_3$ in the ilmenite structure belongs to the space group $R\bar{3}$. The optimized lattice constants are $a = b =$ 5.508 Å, c = 15.818 Å, $\alpha = \beta = 90°$, and $\gamma = 120°$, according to other theoretical and experimental works.[54,55] There is one type of Na and one type of Bi in a $NaBiO_3$ crystal, forming both distorted octahedral clusters (see the Supporting Information file, Figure S2). Both $[NaO_6]$ and $[BiO_6]$ octahedral clusters are distorted with two different bond lengths, where the Na−O bond lengths are longer than the Bi−O bond lengths. Two phases of bismuth oxide (Bi_2O_3) were modeled, β-Bi_2O_3 and δ-Bi_2O_3 polymorphs. β-Bi_2O_3 presents a tetragonal structure belonging to the space group $P42c$ (ICSD 62979) and δ-Bi_2O_3 has a cubic structure belonging to the space group $Fm\bar{3}m$, which was modeled taking into account an occupancy factor of only 0.75 in the 8c Wyckoff positions for the O atoms (ICSD 27458).

$NaBiO_3$ was characterized by X-ray diffraction (XRD) and the corresponding patterns are associated with a hexagonal structure with two hydration molecules ($NaBiO_3{\cdot}2H_2O$), as described by PDF 30-1161[56] in the Joint Committee on Powder Diffraction Standards (JCPDS) database (see the Supporting Information, Figure S1). $NaBiO_3$ crystals have a hexagonal structure belonging to the space group $P3$ with two molecular formula units per unit cell (Z = 2). Because of its low purity (80%), the δ-Bi_2O_3 phase was also present, according to PDF 52-1007[57] in the JCPDS database. These results can be attributed to the fact that $NaBiO_3{\cdot}2H_2O$ is obtained at high temperatures through the oxidation of $Bi(NO_3)_3{\cdot}5H_2O$ by NaOH,[58] and therefore, the hexagonal polymorph of $NaBiO_3$ and cubic polymorph of δ-Bi_2O_3 are obtained.

$NaBiO_3$ was irradiated using an electron beam under high vacuum in a TEM at 200 kV. Figure 1 shows low-magnification

DOI: 10.1021/acs.jpcc.8b11566
J. Phys. Chem. C 2019, 123, 5023−5030

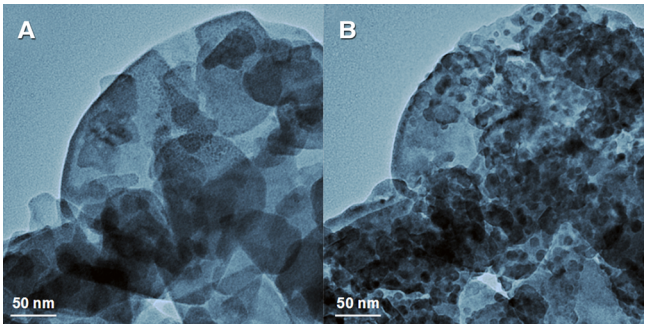

Figure 1. (A) Low-magnification TEM image of the sample before the irradiation by electron beam and (B) after 10 min of exposure to irradiation by electron beam.

TEM images of the material before being irradiated. According to Figure 1B, after 10 min of irradiation with the electron beam, the formation of nanocrystals of Bi could be observed on the surface of the sample.

The effect of exposure time was investigated and the TEM images are displayed in Figure 2A,B,D,E. An analysis of the results suggests that the morphology of the Bi NPs changes with time with the formation of agglomerates with nonregular shapes and diameters of about 10−100 nm. In Figure 1B, it is also possible to observe spheroidal NPs and some particles with morphology of beans or earthworms, like in Figure 2A, which could be associated to the irregular shape of the initial particles or coalescence of some spheroidal NPs as an effect of electron beam irradiation. It can be observed that as the electron irradiation time increases, the Bi NPs perform a coalescence process to form larger particles. At short times of electron irradiation, the formation of NPs of Bi is more slow, while at lower acceleration voltages (5−30 kV that are obtained in scanning electron microscopy), it is observed that the energy of the electron beam is not enough to provoke the reduction of Bi, with this process being dependent on the energy of the electron beam.

Semiquantitative analysis of the EDS data shows that, at first, we have very similar amounts of Na and Bi because of the stoichiometry of the compound. Because δ-Bi_2O_3 is an impurity present in the $NaBiO_3$, a slightly higher amount of Bi was observed at the start of experiments (Figure 2C). After the formation of the agglomerates on the surface of the material and its subsequent degradation, an increase in the amount of Bi (91%) was observed because of the reduction of Bi(V) to metallic Bi (Figure 2F). The Cu and C elements observed in the EDS data are from the sample port. A similar behavior was found by Zheng et al.[59] in their study of the in situ coalescence process of Bi NPs by liquid cell TEM.

High-resolution micrographs (HR-TEM) were taken to analyze the formed nanocrystals (Figure 3). Before irradiation with the electron beam, the (110) plane with an interplanar distance of 2.80 Å (Figure 3B) characteristic of hexagonal $NaBiO_3$[56] was found, and EDS analysis was performed to confirm the presence Na in the material (see Supporting Information, Figure S3). After 10 min of exposure (Figure

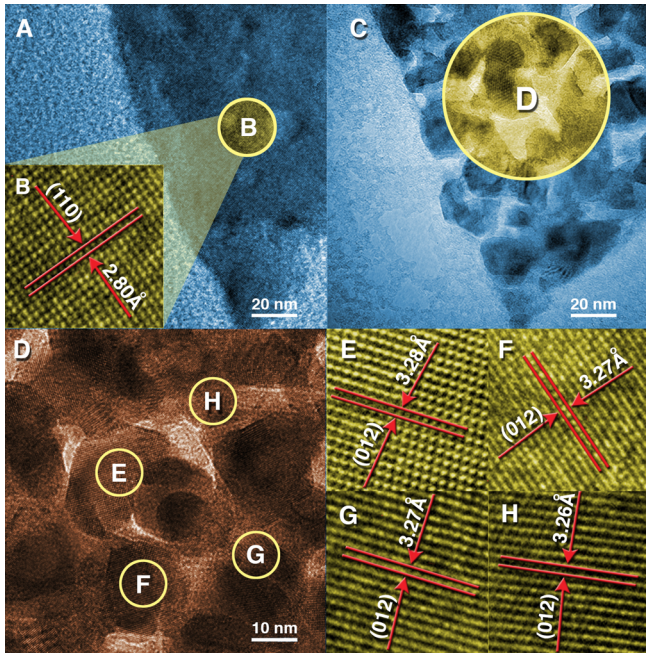

Figure 3. TEM image of the $NaBiO_3$ before (A,B) the irradiation by electron beam and after (C). (D) HR-TEM micrographs at higher magnification (C). (E−H) NPs of Bi rhombohedral.

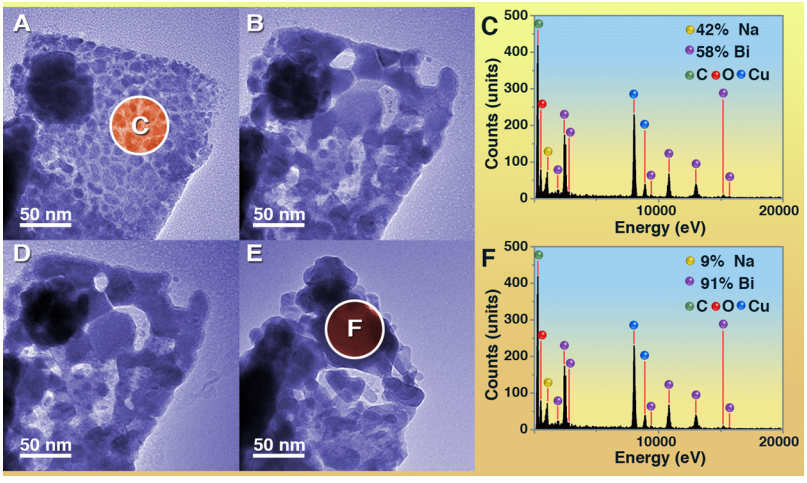

Figure 2. TEM image of the sample after (A) 10, (B) 15, (D) 20, and (E) 30 min of exposure. (C,F) EDS of the white circle in the image and their quantification.

DOI: 10.1021/acs.jpcc.8b11566
J. Phys. Chem. C 2019, 123, 5023−5030

3C,D), small crystalline nonregular clusters appeared, and they were analyzed. The (012) plane with an interplanar distance of 3.28 Å was observed, corresponding to the rhombohedral structure of metallic Bi (Figure 3E−G) associated with PDF 44-1246[60] in the JCPDS database.

Under electron beam irradiation, there is a redistribution of electrons, associated with transitions of electrons from occupied to unoccupied states in the band structure of the crystal. The occupied states in the valence band, VB, are below the Fermi level (quantum stable) and the unoccupied states in the conduction band, CB, are mostly above the Fermi level (unstable states, i.e., quantum excited states). These rearrangements induce oxidation−reduction reactions, and in the present case, the octahedral $[BiO_6]$ cluster of $NaBiO_3$ accumulates an excess of electron density, producing a continuous reduction in the oxidation state of Bi from (V) to zero (metallic Bi), via Bi(III) in Bi_2O_3.

$NaBiO_3$ is an n-type semiconductor. After the electron beam irradiation, the Bi-rich region becomes an n−p-type semiconductor because of the formation of internal defects caused by Bi vacancies in localized areas, thus enhancing the transfer and separation of photo-generated electron−hole pairs. Then, the action of the electron beam of the TEM induces the reduction of Bi cations in $NaBiO_3$ and the subsequent segregation of metallic Bi through the $NaBiO_3$ crystalline lattice. This creates regions with Bi vacancies (V_{Bi}) which function as an n-type semiconductor, and regions with oxygen vacancies (V_O), which function as a p-type semiconductor. The formation of this p−n junction between the xBi/$NaBi_{1-x}O_3$ heterostructure is expected to enhance the reduction activity by enhancing the conductivity, electron mobility, and lifetime of photo-generated electron−hole pairs.

A comparison with the results obtained in our previous paper which Bi NPs are obtained by a femtosecond laser,[38] which renders that the large number of photons generated in a femtosecond laser interacts with $NaBiO_3$ substrate and is capable to produce a plasma with high pressure and temperature values (10^{10} to 10^9 Pa and 1000 K, respectively). These critical conditions allow the three distinct phases of Bi to coexist: rhombohedral, cubic, and tetrahedral. Hence, the present results demonstrate that the experimental conditions from the synthesis using an electron beam of TEM in vacuum can selectively produce the most stable rhombohedral structure of metallic Bi. This experimental observation is also consistent with the literature reporting the formation metallic Bi in a TEM.[39]

To gain a deeper insight into these experimental observations and to provide some basis upon which to understand the effects described above, a detailed theoretical study of the electronic charge of each atom was conducted using Bader charge analysis within the QTAIM framework. Finding zero flux surfaces between two atoms allows the atomic charge to be calculated by integrating the charge density within the atomic basins, Ω, and subtracting the nuclear charge, Z, of the corresponding atom. The charge densities of the Na, Bi, and O centers as a function of the number of electrons added are depicted in Figure 4A and the values are collected in Table S1 of the Supporting Information. In addition, the primitive cell of $NaBiO_3$ without and with the addition of three and eight electrons and the distances from their metallic centers to the corresponding oxygen atoms, that is, the Na−O and Bi−O bond lengths, are presented in Figure 4B. An analysis of Figure 4A shows that the charge density of

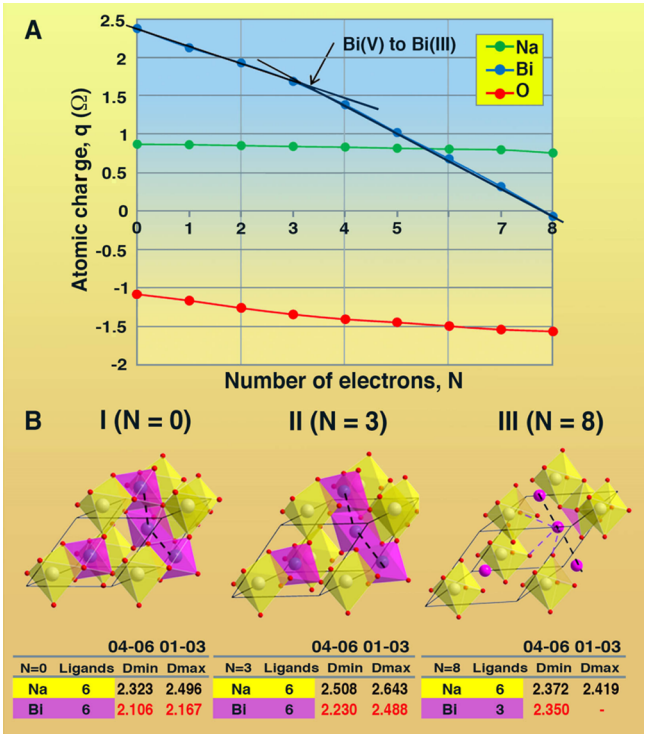

Figure 4. (A) Bader charge density of Bi, Na, and O centers as a function of the number of electrons added. $q(\Omega)$ represents the number of valence electrons minus the calculated charge density; (B) primitive cell without (I) and with the addition of three (II) and eight electrons (III) in $NaBiO_3$ and the minimum and maximum distances in Å (d_{min} and d_{max}, respectively) of the metallic centers to their oxygen atoms.

the Na centers is maintained, whereas the Bi centers of the $[BiO_6]$ clusters show decreasing charge densities with different behavior as electrons are added. From the addition of three electrons onward, the decrease in the Bi charge density becomes more noticeable.

At the same time, the two Bi−O distances start to change after the addition of three electrons, as can be seen in Figure SI4 of the Supporting Information. The pronounced decrease in Bi charge density continues upon increasing N from 4 to 8, in which range only three Bi−O distances were found. It is interesting to note that for the $[NaO_6]$ octahedral clusters, the two Na−O distances remain almost unaltered. These findings suggest a possible decomposition of $NaBiO_3$ into Bi_2O_3, and then the continued reduction of Bi(III) to metallic Bi.

In Figure 5, the variation of the positions of both VB and CB is analyzed along the process of addition of electrons; first, in the neutral $NaBiO_3$ system (N = 0), with the addition of three (N = 3) and eight (N = 8) electrons to visualize the reduction in the oxidation state of Bi from (V) to Bi(III) in Bi_2O_3 and to metallic Bi(zero), respectively. This scheme showed in Figure 5 follows the common case of a heterojunction based on the n-type semiconductor and metal, in which at the interface of the materials electrons flow from the semiconductor into the metal to adjust the Fermi energy levels.

Bader charge analysis for the tetragonal β-Bi_2O_3 and cubic δ-Bi_2O_3 structures was performed, and the results are presented in Figures 6 and 7, respectively. The charge densities of the Bi and O centers as a function of the number of electrons added to β-Bi_2O_3 are depicted in Figure 6A, while its unit cell without and with the addition of 6 and 15 electrons and the distance

DOI: 10.1021/acs.jpcc.8b11566
J. Phys. Chem. C 2019, 123, 5023−5030

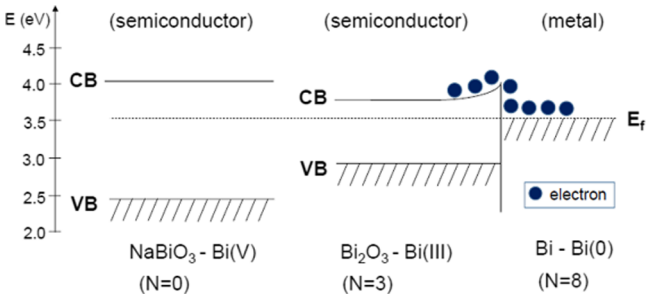

Figure 5. Variation of the positions of VB and CB as a function of the number of electrons added, N. The position of the Fermi energy level, E_f, is placed once the metallic Bi is formed.

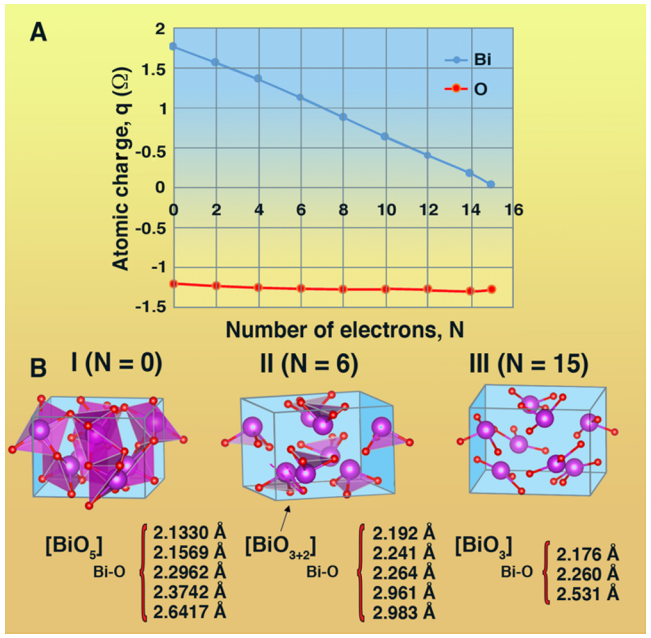

Figure 6. (A) Bader charge density of Bi and O centers as a function of the number of electrons added. (B) Unit cell β-Bi_2O_3 without (I), with the addition of 6 electrons (II) and with the addition of 15 electrons (III); and the Bi−O distances of the structural clusters.

between its metallic centers to the corresponding oxygen anions are presented in Figure 6B. An analysis of the results suggests that the Bi centers of the [BiO_5] clusters decrease their charge density gradually up to six electrons added, at which point the Bi coordination number changes and is reduced to three. After the addition of six electrons, the coordination was maintained while the Bi−O distance increased up to 2.531 Å for N = 15, where the Bi atom was completely reduced (Figure S5). The charge density of the Bi and O centers as a function of the number of electrons added to δ-Bi_2O_3 is presented in Figure 7A, while its cubic unit cell without and with the addition of eight electrons is shown in Figure 7B. Bi centers of the cabin-type [BiO_6] clusters showed gradually decreasing charge densities up to the addition of eight electrons, at which point the Bi atom was completely reduced, keeping the Bi coordination. At this point, the Bi−O distance increased from 2.394 to 2.842 Å because of the cell expansion (Figure S5). The charge density values of Na, Bi, and O centers for β-Bi_2O_3 and δ-Bi_2O_3 structures are collected in Table S2 of the Supporting Information.

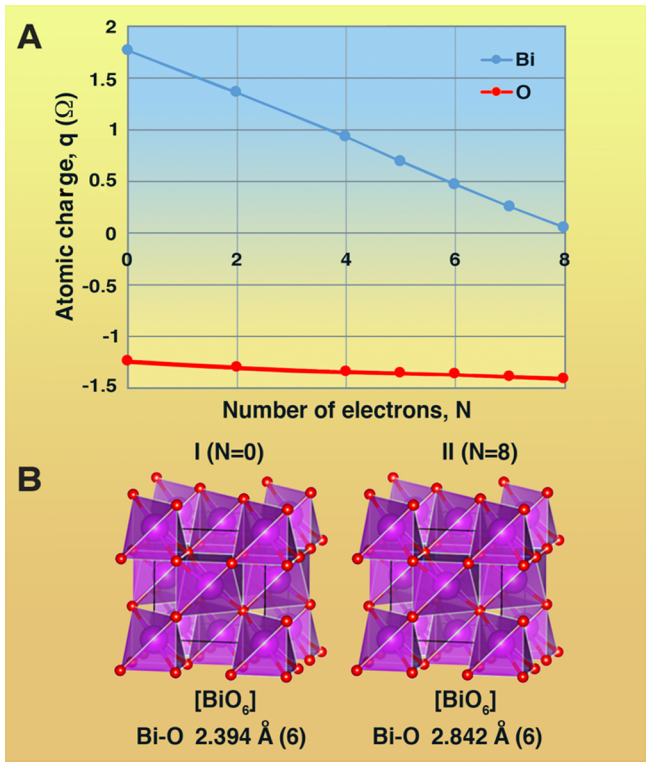

Figure 7. (A) Bader charge density of Bi and O centers as a function of the number of electrons added. (B) Unit cell δ-Bi_2O_3 without (I) and with the addition of eight electrons (II); and the Bi−O distances of the structural clusters.

As the transition from Bi(III) to metallic Bi was not observed during the reduction of $NaBiO_3$, the same study was performed using β-Bi_2O_3 as the starting reagent (Figure 8). The sample was taken to the TEM and exposed to the electron

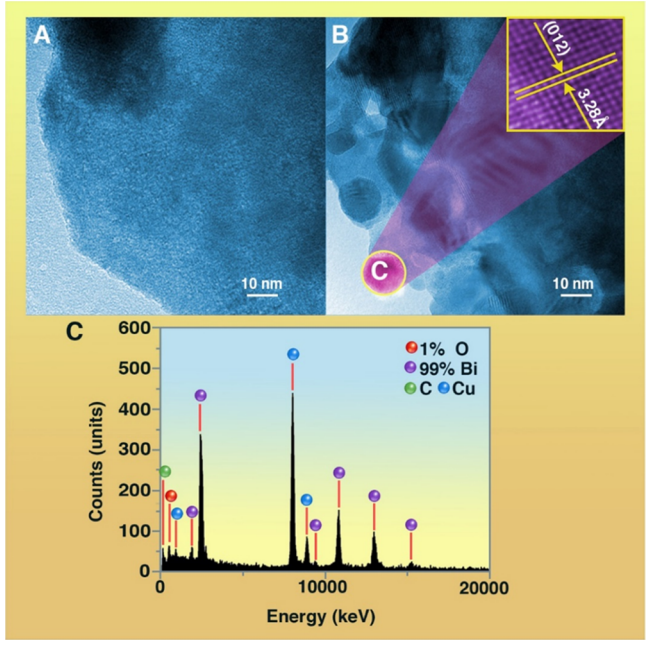

Figure 8. (A) TEM image of the β-Bi_2O_3 before the irradiation by electron beam and (B) after 15 min exposure. (C) EDS of the yellow circle in the image and their quantification.

DOI: 10.1021/acs.jpcc.8b11566
J. Phys. Chem. C 2019, 123, 5023−5030

beam. After 15 min of exposure, crystalline clusters started to appear on the surface of the β-Bi_2O_3, as seen in $NaBiO_3$. These NPs were characterized as rhombohedral metallic Bi based on observation of the (012) plane with an interplanar distance of 3.28 Å (Figure 8B), similar to the results obtained for $NaBiO_3$. The EDS analysis showed that the NPs that appeared on the surface were formed of Bi (99%), proving that β-Bi_2O_3 undergoes the process of reduction from Bi(III) to metallic Bi (Figure 8C).

4. CONCLUSIONS

During the process of TEM observation (interaction of an electron beam with matter), some novel phenomena were discovered. These interactions can be used to fabricate NPs and investigate their structure and chemical transformation, which is of importance for the development of novel nanostructures, especially for those that cannot be obtained using conventional chemical and physical methods.

In this work, we studied the in situ crystal growth of pure single crystals of metallic Bi on the surface of $NaBiO_3$, δ-Bi_2O_3, and β-Bi_2O_3 under the electron beam of an FE-TEM. First-principles calculations at the DFT level and QTAIM analysis were combined with different characterization techniques, including HR-TEM and EDS to extend our fundamental understanding of the atomic processes that underpin the formation of Bi NPs on these materials mediated by electron beam irradiation.

The main conclusions of the present work can be summarized as follows: (i) both theoretical and experimental findings can be used to find a relationship between atomic-scale structural and electronic perturbations induced by electron beam irradiation, providing adequate conditions for the formation of Bi NPs on $NaBiO_3$; (ii) electron beam irradiation can induce the breaking of Bi−O, and to a lesser extent Na−O, bonds in the $[BiO_6]$ and $[NaO_6]$ clusters, respectively, as constituent building blocks of $NaBiO_3$; (iii) under electron beam irradiation, a redistribution of electrons takes place with a concomitant reduction in the oxidation state of Bi from (V) to zero (metallic Bi); (iv) first, the formation of β-Bi_2O_3, with a Bi(III) oxidation state, takes place followed by the subsequent appearance of metallic Bi NPs; and (v) these structural and electronic perturbations of the material provoke a change from n-type to p-type semiconductor behavior associated with the formation of a p−n xBi/$NaBi_{1-x}O_3$ heterostructure.

With the use of robust experimental and theoretical tools, scientists now have the capability to push the limits of investigation to the ultimate level of individual atoms and single bonds. If this knowledge can be transformed to develop useful NPs, then exciting opportunities to engineer novel assemblies for new applications are wide open. The current work sheds light on the potential use of electron beams to trigger the formation of Bi and other metal NPs.

■ ASSOCIATED CONTENT

Supporting Information

The Supporting Information is available free of charge on the ACS Publications website at DOI: 10.1021/acs.jpcc.8b11566.

XRD patters for commercial $NaBiO_3$; conventional and primitive cell of $NaBiO_3$ in the rhombohedral space group $R\bar{3}$ EDS analysis of $NaBiO_3$; variation of Bi−O distances and of cell parameters in $NaBiO_3$ structure as a function of the number of electrons added, N; and variation of cell parameters in Bi_2O_3 structure as a function of the number of electrons added, N. (A) β-Bi_2O_3 and (B) δ-Bi_2O_3 (PDF)

■ AUTHOR INFORMATION

Corresponding Author

*E-mail: andres@qfa.uji.es. Phone: 0034964728083. Fax: 0034964728066.

ORCID

Marcelo Assis: 0000-0003-0355-5565
Thales Rafael Machado: 0000-0002-3246-6329
Nadia Guerra Macedo: 0000-0001-7031-2729
João Paulo Campos Costa: 0000-0002-7366-6829
Juan Andrés: 0000-0003-0232-3957
Elson Longo: 0000-0001-8062-7791

Notes

The authors declare no competing financial interest.

■ ACKNOWLEDGMENTS

The authors acknowledge the financial support of agencies: Coordenação de Aperfeiçoamento de Pessoal de Nível Superior—Brazil (CAPES)—Finance code 001—PNPD program, FINEP, FAPESP (2013/07296-2, 2013/26671-9), CNPq (166281/2017-4), Generalitat Valenciana for PrometeoII/2014/022, ACOMP/2015/1202, Ministerio de Economia y Competitividad, project CTQ2015-65207-P, and Universitat Jaume I" project no. UJI-B2016-25. The authors thank Enio Longo for the support with the scientific illustrations. The authors also thank the Servei d'Informàtica, Universitat Jaume I, for generous allocation of computer time.

■ REFERENCES

(1) Gonzalez-Martinez, I. G.; Bachmatiuk, A.; Bezugly, V.; Kunstmann, J.; Gemming, T.; Liu, Z.; Cuniberti, G.; Rümmeli, M. H. Electron-Beam Induced Synthesis of Nanostructures: A Review. *Nanoscale* **2016**, *8*, 11340−11362.

(2) Zhang, W.; Zheng, W. T. Transmission Electron Microscopy Finds Plenty of Room on the Surface. *Phys. Chem. Chem. Phys.* **2015**, *17*, 14461−14469.

(3) Williams, D. B.; Carter, C. B. *Transmission Electron Microscopy: a Textbook for Materials Science*; Springer: New York, 2009.

(4) Xu, Y.; Shi, L.; Zhang, X.; Wong, K.; Li, Q. The electron beam irradiation damage on nanomaterials synthesized by hydrothermal and thermal evaporation methods-An example of ZnS nanostructures. *Micron* **2011**, *42*, 290−298.

(5) Yen, M.-Y.; Chiu, C.-W.; Chen, F.-R.; Kai, J.-J.; Lee, C.-Y.; Chiu, H.-T. Convergent Electron Beam Induced Growth of Copper Nanostructures: Evidence of the Importance of a Soft Template. *Langmuir* **2004**, *20*, 279−281.

(6) Tham, D.; Nam, C.-Y.; Fischer, J. E. Microstructure and Composition of Focused-Ion-Beam-Deposited Pt Contacts to GaN Nanowires. *Adv. Mater.* **2006**, *18*, 290−294.

(7) Liao, H.-G.; Niu, K.; Zheng, H. Observation of Growth of Metal Nanoparticles. *Chem. Commun.* **2013**, *49*, 11720−11727.

(8) Moser, T. H.; Mehta, H.; Park, C.; Kelly, R. T.; Shokuhfar, T.; Evans, J. E. The Role of Electron Irradiation History in Liquid Cell Transmission Electron Mycroscopy. *Sci. Adv.* **2018**, *4*, No. eaaq1202.

(9) Mirsaidov, U. M.; Zheng, H.; Bhattacharya, D.; Casana, Y.; Matsudaira, P. Direct Observation of Stick-slip Movements of Water Nanodroplets Induced by an Electron Beam. *Proc. Natl. Acad. Sci. U.S.A.* **2012**, *109*, 7187−7190.

DOI: 10.1021/acs.jpcc.8b11566
J. Phys. Chem. C 2019, 123, 5023−5030

(10) Böhler, E.; Warneke, J.; Swiderek, P. Control of Chemical Reactions and Synthesis by Low-energy Electrons. *Chem. Soc. Rev.* **2013**, *42*, 9219−9231.
(11) Su, Q.; Li, J.; Zhong, G.; Du, G.; Xu, B. In Situ Synthesis of Iron/Nickel Sulfide Nanostructures-Filled Carbon Nanotubes and Their Electromagnetic and Microwave-Absorbing Properties. *J. Phys. Chem. C* **2011**, *115*, 1838−1842.
(12) Hu, J.; Sun, Y.; Chen, Z. Rapid Fabrication of Nanocrystals Through In Situ Electron Beam Irradiation in a Transmission Electron Microscope. *J. Phys. Chem. C* **2009**, *113*, 5201−5205.
(13) Zhu, Y. T.; Liao, X. Retaining ductility. *Nat. Mater.* **2004**, *3*, 351−352.
(14) Lee, J.-S.; Kovalenko, M. V.; Huang, J.; Chung, D. S.; Talapin, D. V. Band-like Transport, High Electron Mobility and High Photoconductivity in All-Inorganic Nanocrystal Arrays. *Nat. Nanotechnol.* **2011**, *6*, 348−352.
(15) Yamada, Y.; Tsung, C.-K.; Huang, W.; Huo, Z.; Habas, S. E.; Soejima, T.; Aliaga, C. E.; Somorjai, G. A.; Yang, P. Nanocrystal Bilayer for Tandem Catalysis. *Nat. Chem.* **2011**, *3*, 372−376.
(16) Lim, D.-W.; Yoon, J. W.; Ryu, K. Y.; Suh, M. P. Magnesium Nanocrystals Embedded in a Metal-Organic Framework: Hybrid Hydrogen Storage with Synergistic Effect on Physi- and Chemisorption. *Angew. Chem., Int. Ed.* **2012**, *51*, 9814−9817.
(17) Wu, P.; Yan, X.-P. Doped Quantum Dots for Chemo/Biosensing and Bioimaging. *Chem. Soc. Rev.* **2013**, *42*, 5489−5521.
(18) Cargnello, M.; Doan-Nguyen, V. V. T.; Gordon, T. R.; Diaz, R. E.; Stach, E. A.; Gorte, R. J.; Fornasiero, P.; Murray, C. B. Control of Metal Nanocrystal Size Reveals Metal-Support Interface Role for Ceria Catalysts. *Science* **2013**, *341*, 771−773.
(19) Longo, V. M.; De Foggi, C. C.; Ferrer, M. M.; Gouveia, A. F.; André, R. S.; Avansi, W.; Vergani, C. E.; Machado, A. L.; Andrés, J.; Cavalcante, L. S.; et al. Potentiated Electron Transference in Alpha-Ag_2WO_4 Microcrystals with Ag Nanofilaments as Microbial Agent. *J. Phys. Chem. A* **2014**, *118*, 5769−5778.
(20) Wang, Q. P.; Guo, X. X.; Wu, W. H.; Liu, S. X. Preparation of Fine Ag_2WO_4 Antibacterial Powders and Its Application in the Sanitary Ceramics. *Adv. Mater. Res.* **2011**, *284-286*, 1321−1325.
(21) Roca, R. A.; Sczancoski, J. C.; Nogueira, I. C.; Fabbro, M. T.; Alves, H. C.; Gracia, L.; Santos, L. P. S.; de Sousa, C. P.; Andrés, J.; Luz, G. E.; et al. Facet-Dependent Photocatalytic and Antibacterial Properties of α-Ag_2WO_4 Crystals: Combining Experimental Data and Theoretical Insights. *Catal. Sci. Technol.* **2015**, *5*, 4091−4107.
(22) Longo, E.; Cavalcante, L. S.; Volanti, D. P.; Gouveia, A. F.; Longo, V. M.; Varela, J. A.; Orlandi, M. O.; Andrés, J. Direct in situ Observation of the Electron-driven Synthesis of Ag Filaments on Alpha-Ag_2WO_4 Crystals. *Sci. Rep.* **2013**, *3*, 1676.
(23) Andrés, J.; Gracia, L.; Gonzalez-Navarrete, P.; Longo, V. M.; Avansi, W., Jr.; Volanti, D. P.; Ferrer, M. M.; Lemos, P. S.; La Porta, F. A.; Hernandes, A. C.; et al. Structural and Electronic Analysis of the Atomic Scale Nucleation of Ag on alpha-Ag_2WO_4 Induced by Electron Irradiation. *Sci. Rep.* **2014**, *4*, 5391.
(24) da Silva Pereira, W.; Andrés, J.; Gracia, L.; San-Miguel, M. A.; da Silva, E. Z.; Longo, E.; Longo, V. M. Elucidating the Real-time Ag Nanoparticle Growth on α-Ag_2WO_4 During Electron Beam Irradiation: Experimental Evidence and Theoretical Insights. *Phys. Chem. Chem. Phys.* **2015**, *17*, 5352−5359.
(25) Longo, E.; Volanti, D. P.; Longo, V. M.; Gracia, L.; Nogueira, I. C.; Almeida, M. A. P.; Pinheiro, A. N.; Ferrer, M. M.; Cavalcante, L. S.; Andrés, J. Toward an Understanding of the Growth of Ag Filaments on α-Ag_2WO_4 and their Photoluminescent Properties: A Combined Experimental and Theoretical Study. *J. Phys. Chem. C* **2014**, *118*, 1229−1239.
(26) San-Miguel, M. A.; da Silva, E. Z.; Zanetti, S. M.; Cilense, M.; Fabbro, M. T.; Gracia, L.; Andrés, J.; Longo, E. In situ Growth of Ag Nanoparticles on alpha-Ag_2WO_4 under Electron Irradiation: Probing the Physical Principles. *Nanotechnology* **2016**, *27*, 225703.
(27) Longo, E.; Avansi, W., Jr.; Bettini, J.; Andres, J.; Gracia, L. In situ Transmission Electron Microscopy Observation of Ag Nanocrystal Evolution by Surfactant Free Electron-driven Synthesis. *Sci. Rep.* **2016**, *6*, 21498.
(28) Roca, R. A.; Gouveia, A. F.; Lemos, P. S.; Gracia, L.; Andrés, J.; Longo, E. Formation of Ag Nanoparticles on β-Ag_2WO_4 through Electron Beam Irradiation: A Synergetic Computational and Experimental Study. *Inorg. Chem.* **2016**, *55*, 8661−8671.
(29) Roca, R. A.; Lemos, P. S.; Gracia, L.; Andrés, J.; Longo, E. Uncovering the Metastable ã-Ag_2WO_4 Phase: a Joint Experimental and Theoretical Study. *RSC Adv.* **2017**, *7*, 5610−5620.
(30) Fabbro, M. T.; Gracia, L.; Silva, G. S.; Santos, L. P. S.; Andrés, J.; Cordoncillo, E.; Longo, E. Understanding the Formation and Growth of Ag Nanoparticles on Silver Chromate Induced by Electron Irradiation in Electron Microscope: A Combined Experimental and Theoretical Study. *J. Solid State Chem.* **2016**, *239*, 220−227.
(31) Fabbro, M. T.; Saliby, C.; Rios, L. R.; La Porta, F. A.; Gracia, L.; Li, M. S.; Andrés, J.; Santos, L. P. S.; Longo, E. Identifying and Rationalizing the Morphological, Structural, and Optical Properties of β-Ag_2MoO_4 Microcrystals, and the Formation Process of Ag Nanoparticles on their Surfaces: Combining Experimental Data and First-Principles Calculations. *Sci. Technol. Adv. Mater.* **2016**, *16*, 065002.
(32) de Oliveira, R. C.; Assis, M.; Teixeira, M. M.; da Silva, M. D. P.; Li, M. S.; Andres, J.; Gracia, L.; Longo, E. An Experimental and Computational Study of β-$AgVO_3$: Optical Properties and Formation of Ag Nanoparticles. *J. Phys. Chem. C* **2016**, *120*, 12254−12264.
(33) Botelho, G.; Sczancoski, J. C.; Andres, J.; Gracia, L.; Longo, E. Experimental and Theoretical Study on the Structure, Optical Properties, and Growth of Metallic Silver Nanostructures in Ag_3PO_4. *J. Phys. Chem. C* **2015**, *119*, 6293−6306.
(34) Ghatak, J.; Guan, W.; Möbus, G. In Situ TEM Observation of Lithium Nanoparticle Growth and Morphological Cycling. *Nanoscale* **2012**, *4*, 1754−1759.
(35) Ito, Y.; Jain, H.; Williams, D. B. Electron-Beam Induced Growth of Cu Nanoparticles in Silica Glass Matrix. *Appl. Phys. Lett.* **1999**, *75*, 3793−3795.
(36) Yang, Z.; Walls, M.; Lisiecki, I.; Pileni, M.-P. Unusual Effect of an Electron Beam on the Formation of Core/Shell (Co/CoO) Nanoparticles Differing by Their Crystalline Structures. *Chem. Mater.* **2013**, *25*, 2372−2377.
(37) Hermannsdörfer, J.; de Jonge, N.; Verch, A. Electron Beam Induced Chemistry of Gold Nanoparticles in Saline Solution. *Chem. Commun.* **2015**, *51*, 16393−16396.
(38) Assis, M.; Cordoncillo, E.; Torres-Mendita, R.; Beltrán-Mir, H.; Mínguez-Vega, G.; Gouveia, A. F.; Leite, E.; Andrés, J.; Longo, E. Laser-induced formation of bismuth nanoparticles. *Phys. Chem. Chem. Phys.* **2018**, *20*, 13693−13696.
(39) Sepulveda-Guzman, S.; Elizondo-Villarreal, N.; Ferrer, D.; Torres-Castro, A.; Gao, X.; Zhou, J. P.; Jose-Yacaman, M. In situformation of bismuth nanoparticles through electron-beam irradiation in a transmission electron microscope. *Nanotechnology* **2007**, *18*, 335604.
(40) Liu, L.; Wang, H.; Yi, Z.; Deng, Q.; Lin, Z.; Zhang, X. In situ Investigation of Bismuth Nanoparticles Formation by Transmission Electron Microscope. *Micron* **2018**, *105*, 30−34.
(41) Li, J.; Chen, J.; Wang, H.; Chen, N.; Wang, Z.; Guo, L.; Deepak, F. L. In Situ Atomic-Scale Study of Particle-Mediated Nucleation and Growth in Amorphous Bismuth to Nanocrystal Phase Transformation. *Adv. Sci.* **2018**, *5*, 1700992.
(42) Flores-Castañeda, M.; Camps, E.; Camacho-López, M.; Muhl, S.; García, E.; Figueroa, M. Bismuth Nanoparticles Synthesized by Laser Ablation in Lubricant Oils for Tribological Tests. *J. Alloys Compd.* **2015**, *643*, S67−S70.
(43) Torrisi, L.; Silipigni, L.; Restuccia, N.; Cuzzocrea, S.; Cutroneo, M.; Barreca, F.; Fazio, B.; Di Marco, G.; Guglielmino, S. Laser-Generated Bismuth Nanoparticles for Applications in Imaging and Radiotherapy. *J. Phys. Chem. Solids* **2018**, *119*, 62−70.
(44) Escobar-Alarcón, L.; Velarde Granados, E.; Sanchez, D. V.; Olea-Mejia, O.; Haro-Poniatowski, E.; Castañeda, A. A.; Solis-

DOI: 10.1021/acs.jpcc.8b11566
J. Phys. Chem. C 2019, 123, 5023−5030

Casados, D. A. Bismuth and Gold Nanoparticles Prepared by Laser Ablation in Aqueous Solutions. *Adv. Mater. Res.* **2014**, *976*, 196−201.
(45) Kresse, G.; Hafner, J. Ab initiomolecular-dynamics simulation of the liquid-metal-amorphous-semiconductor transition in germanium. *Phys. Rev. B: Condens. Matter Mater. Phys.* **1994**, *49*, 14251−14269.
(46) Perdew, J. P.; Burke, K.; Ernzerhof, M. Generalized Gradient Approximation Made Simple. *Phys. Rev. Lett.* **1996**, *77*, 3865−3868.
(47) Kresse, G. J.; Joubert, D. From Ultrasoft Pseudopotentials to The Projector Augmented-wave Method. *Phys. Rev. B: Condens. Matter Mater. Phys.* **1999**, *59*, 1759−1775.
(48) Dudarev, S. L.; Botton, G. A.; Savrasov, S. Y.; Humphreys, C. J.; Sutton, A. P. Electron-energy-loss spectra and the structural stability of nickel oxide: An LSDA+U study. *Phys. Rev. B: Condens. Matter Mater. Phys.* **1998**, *57*, 1505−1509.
(49) Bader, R. F. W. *Atoms in Molecules: A Quantum Theory*; Oxford University Press: Oxford, 1990.
(50) Matta, C. F.; Boyd, R. J. An Introduction to the Quantum Theory of Atoms in Molecules. *The Quantum Theory of Atoms and Molecules: From Solid State to DNA and Drug Design*; Wiley-VCH Verlag GmbH & Co. KGaA: Weinheim, 2007.
(51) Popelier, P. L. A.; Aicken, F. M.; O'Brien, S. E. *Chemical Modelling: Applications and Theory*; RCS: London, 2000.
(52) Andrés, J.; Gracia, L.; Gouveia, A. F.; Ferrer, M. M.; Longo, E. Effects of Surface Stability on the Morphological Transformation of Metals and Metal Oxides as Investigated by First-Principles Calculations. *Nanotechnology* **2015**, *26*, 405703.
(53) Botelho, G.; Sczancoski, J. C.; Andres, J.; Gracia, L.; Longo, E. Experimental and Theoretical Study on the Structure, Optical Properties, and Growth of Metallic Silver Nanostructures in Ag3PO4. *J. Phys. Chem. C* **2015**, *119*, 6293−6306.
(54) Liu, J.; Chen, S.; Liu, Q.; Zhu, Y.; Zhang, J. Correlation of crystal structures and electronic structures with visible light photocatalytic properties of NaBiO3. *Chem. Phys. Lett.* **2013**, *572*, 101−105.
(55) Kumada, N.; Kinomura, N.; Sleight, A. W. Neutron powder diffraction refinement of ilmenite-type bismuth oxides: ABiO3 (A = Na, Ag). *Mater. Res. Bull.* **2000**, *35*, 2397−2402.
(56) Aurivillius, B.; Malmström, B. G.; Haraldsen, H.; Prydz, H. X-Ray Studies on "Sodium Metabismuthate". *Acta Chem. Scand.* **1955**, *9*, 1219−1221.
(57) Sillén, L. G. *X-Ray Studies on Bismuth Trioxide*; Ark. Kemi, Mineral. Geol., 1937; Vol. *12A*, pp 1−15.
(58) Irmawati, R.; Noorfarizan Nasriah, M. N.; Taufiq-Yap, Y. H.; Abdul Hamid, S. B. Characterization of Bismuth Oxide Catalysts Prepared from Bismuth Trinitrate Pentahydrate: Influence of Bismuth Concentration. *Catal. Today* **2004**, *93-95*, 701−709.
(59) Niu, K.-Y.; Liao, H.-G.; Zheng, H. Visualization of the Coalescence of Bismuth Nanoparticles. *Microsc. Microanal.* **2014**, *20*, 416−424.
(60) Sailer, R.; McCarthy, G. *ICDD Grant-in-Aid*; North Dakota State University: Fargo, North Dakota, USA, 1992.

DOI: 10.1021/acs.jpcc.8b11566
J. Phys. Chem. C 2019, 123, 5023−5030